

Quantum Monte Carlo description of correlated electrons in two-dimensional FeSe

Sam Azadi,^{1,*} A. Principi,¹ R. V. Belosludov,² T. D. Kühne,^{3,4,5} and M. S. Bahramy¹

¹*Department of Physics and Astronomy, University of Manchester,
Oxford Road, Manchester M13 9PL, United Kingdom*

²*Institute for Materials Research, Tohoku University, Sendai 980-08577, Japan*

³*Center for Advanced Systems Understanding, Untermarkt 20, D-02826 Görlitz, Germany*

⁴*Helmholtz Zentrum Dresden-Rossendorf, Bautzner Landstraße 400, D-01328 Dresden, Germany*

⁵*TU Dresden, Institute of Artificial Intelligence, Chair of Computational System Sciences,
Nöthnitzer Straße 46 D-01187 Dresden, Germany*

(Dated: June 10, 2025)

Electronic correlation effects on the structural properties of double-layer FeSe are studied using variation and diffusion quantum Monte Carlo methods. The Slater-Jastrow many-body wavefunction with two different forms for the homogeneous two-body pair-correlation term is used. The ground-state energy of the system is obtained at the thermodynamic limit using two different trial wave functions called JDFT and JSD. Only the Jastrow factor is fully optimized in the JDFT wave function, while the Slater determinant comes from the density functional approximation. In the JSD trial wave function, the Slater determinant and the Jastrow factor are fully optimized simultaneously. We calculated the VMC and DMC energies as a function of interlayer separation for two different in-plane iron-iron bond lengths. Our QMC results indicate that the optimized interlayer separation decreases with increasing iron-iron bond length driven by stretch. We found that a three- to two-dimensional phase transition increases the electron-electron correlation effects and shifts the system from moderately correlated to strongly correlated. The value of correlation energy implies that the Hubbard U value, which is widely used in DFT+U calculations, for two-dimensional FeSe is larger than its value in bulk.

I. INTRODUCTION

The electron-electron (el-el) many-body correlations in magnetic two-dimensional (2D) systems, including iron-based superconductors (FeSCs), play a fundamental role in understanding their structural, magnetic and exotic electronic properties such as unconventional superconductivity [1–7]. In two-dimensional FeSCs, electronic interactions are moderately strong, placing them in an intermediate coupling regime between weak coupling and strong correlation effects found in cuprates[8]. The confinement of electrons in two-dimensional FeSCs enhances correlation effects due to the reduced screening of Coulomb interactions between electrons that introduce magnetic anisotropy, which can be tuned externally by electric fields, strain, photoexcitation, and chemical doping[4, 9–13]. Renormalization of the electronic band structure and the increase in the effective mass of electrons, which is observed in angle-resolved photoemission spectroscopy (ARPES) and quantum oscillation experiments[14], can be enhanced by the el-el correlation interaction. Deviations from Fermi-liquid behavior [15, 16] in FeSCs are introduced by electronic correlations, especially near quantum critical points where magnetic fluctuations dominate. This non-Fermi liquid behavior is reflected in unusual temperature-dependent properties $\rho \sim T^n, n > 2$ and other anomalous properties [17]. Competing orders, such as charge density waves or nematic order, which often coexist or compete with superconductivity, can be stabilized due to correlation effects[18–20]. Nematicity, characterized by the break of rotational symmetry, is strongly influenced by many-body el-el correlations in FeSCs[21]. Two-dimensional FeSCs provide an ideal platform for studying the interplay between electron correlations and reduced dimensionality, bridging the gap between weakly correlated systems (such as conventional superconductors) and strongly correlated systems (such as cuprates) [1, 2, 4, 10]. In this work, many-body el-el correlations in two-dimensional iron selenide (2D-FeSe) are calculated using continuous quantum Monte Carlo methods in real space.

Two-dimensional iron selenide (2D-FeSe) provides a versatile platform for exploring quantum phenomena and exotic phases of matter within the family of iron-based superconductors [10, 22–26]. 2D-FeSe exhibits unique electronic and magnetic behaviors, even within the one-particle approach [27], suggesting a complex interplay between nematicity, magnetism, and superconductivity[19]. The bulk FeSe undergoes a structural phase transformation from tetragonal to orthorhombic at approximately ~ 90 K [22, 28, 29], without any finite magnetic order under ambient conditions.

* sam.azadi@manchester.ac.uk

Its critical superconducting transition temperature is ~ 8 K [28], which can increase to ~ 37 K under a hydrostatic pressure of ~ 6 GPa [7, 30]. Correlation interactions significantly renormalize electronic bands in FeSe and enhance effective masses by factors $\sim 3\text{--}5$ compared to band theory predictions[31]. Bulk FeSe undergoes a nematic phase transition at ~ 90 K, breaking the rotational symmetry of the crystal and electronic structure, driven by orbital-dependent electronic correlations, with a strong interaction between orbitals d_{xz} and d_{yz} [22]. However, in 2D-FeSe, the nematic phase can be suppressed, possibly due to enhanced quantum fluctuations that may contribute to the high T_c by shifting the balance between competing orders[32].

In this work, we focus on double-layer 2D-FeSe, its electronic properties can be influenced by interlayer separation, which is governed by long-range van der Waals (vdW) interactions [33]. Controlling this separation, for example, through isothermal compression, allows tuning of various emergent features, such as the coupling between nematicity and magnetism [12]. The coexistence of competing orders, namely weak vdW forces and strong localized interactions in double-layer 2D-FeSe system, presents unique opportunities to explore exotic quantum phenomena, with implications for both fundamental science and technological applications. Our main tools are real space variation and diffusion quantum Monte Carlo methods which can accurately describe the correlation driven phenomena.

Real-space Variational Quantum Monte Carlo (VMC) and Diffusion Quantum Monte Carlo (DMC) have proven to be highly successful in studying electronic correlation effects in transition metal compounds and capturing weak vdW interaction[34–37], including systems like FeSe[38], due to the fact that they directly address the many-body nature of electron interactions, which are critical in correlated systems with partially filled d -orbitals. Traditional mean-field approaches, such as density functional theory (DFT) with local density approximation (LDA) or generalized gradient approximation (GGA), often fail to capture strong correlations. VMC and DMC go beyond mean-field approximations by directly solving the many-body Schrödinger equation using the stochastic techniques. Both VMC and DMC allow for systematic improvement of accuracy by refining trial wave functions and optimizing variational parameters using variance and energy minimization[39].

In variational Monte Carlo (VMC) calculations, the expectation value of a many-electron Hamiltonian is calculated with respect to a trial wave function (WF) that can be of arbitrary complexity [40, 41]. In diffusion Monte Carlo (DMC) simulations, we simulate a process controlled by the Schrödinger equation in imaginary time to project out the ground-state component of an initial WF. We use the fixed-node approximation to impose fermionic antisymmetry [42]. VMC provides detailed insights into the role of electronic correlations by using explicitly many-body-correlated trial wavefunctions with well-optimized Jastrow factors. DMC improves upon VMC by stochastically projecting the trial wave function onto the exact ground-state wavefunction, minimizing errors from the trial wave function. DMC is one of the most accurate methods for strongly correlated systems.

II. METHOD

The main ingredient of our QMC calculations is the many-body wavefunction with the resonance value bond (RVB) format defined as the product of a Jastrow factor J and an antisymmetrized geminal power (AGP) determinant part Ψ_{AGP} [27, 43] as implemented in TurboRVB[44]. The determinant part is:

$$\Psi_{\text{AGP}}(\mathbf{R}) = \mathcal{A} \prod_{i=1}^{N_{\downarrow}} \phi(\mathbf{r}_i^{\uparrow}, \mathbf{r}_i^{\downarrow}) \quad (1)$$

where \mathcal{A} , $\mathbf{R} = \{\mathbf{r}_1^{\uparrow}, \dots, \mathbf{r}_{N_{\uparrow}}^{\uparrow}, \mathbf{r}_1^{\downarrow}, \dots, \mathbf{r}_{N_{\downarrow}}^{\downarrow}\}$, and $\phi(\mathbf{r}_i^{\uparrow}, \mathbf{r}_i^{\downarrow}) = \phi(\mathbf{r}_i^{\downarrow}, \mathbf{r}_i^{\uparrow})$, are the antisymmetrization operator, the $3N$ -dimensional vector of electron coordinates, and a symmetric orbital function describing the singlet pairs, respectively. N , N_{\uparrow} and N_{\downarrow} are the total number of electrons, spin-up and spin-down electrons, respectively $N_{\uparrow} = N_{\downarrow} = N/2$. The pairing function in eq. 1 is expanded in terms of molecular orbitals (MOs)

$$\phi(\mathbf{r}^{\uparrow}, \mathbf{r}^{\downarrow}) = \sum_{i=1}^{N/2} \alpha_i \psi_i^{\text{MO}}(\mathbf{r}^{\uparrow}) \psi_i^{\text{MO}}(\mathbf{r}^{\downarrow}), \quad (2)$$

The MOs are expanded in a Gaussian single-particle basis set χ centered on the atomic position $\psi_i^{\text{MO}}(\mathbf{r}) = \sum_j \beta_{ij} \chi_j(\mathbf{r})$ [43, 45]. If not mentioned, our results are obtained using an uncontracted Gaussian basis of $8s6p4d1f$ and $6s4p2d$ orbitals for Fe and Se, respectively. Initial values of the Gaussian orbitals chosen from the cc-pVTZ [46] basis set. The core electrons of the Fe and Se atoms were replaced by correlation consistent effective core potentials (ccECPs)[47, 48]. Our simulation cell is subject to two-dimensional periodic boundary conditions in the xy direction with standard Ewald summations to calculate the Coulomb interaction. The variational parameters in our AGP wave function are α_i , β_{ij} , and the exponents of the uncontracted Gaussian basis set χ . The initial MOs were obtained using the density functional approach [49] with the local density approximation (LDA) [50] using the same uncontracted Gaussian basis set described above.

N	$VMC-J_F DFT$	$DMC-J_F DFT$	$VMC-J_F SD$	$DMC-J_F SD$	$VMC-J_C DFT$	$DMC-J_C DFT$	$VMC-J_C SD$	$DMC-J_C SD$
176	-6.022123(8)	-6.03398(3)	-6.029479(6)	-6.03741(3)	-6.021325(8)	-6.033809(4)	-6.029264(6)	-6.03740(2)
396	-6.020526(9)	-6.03299(5)	-6.027806(7)	-6.03603(4)	-6.019759(9)	-6.032964(6)	-6.027308(7)	-6.03624(4)
704	-6.02007(1)	-6.03254(8)	-6.026830(9)	-6.03519(8)	-6.01904(2)	-6.03235(8)	-6.02627(1)	-6.03547(9)
∞	-6.01934(1)	-6.0321(1)	-6.02611(1)	-6.0346(2)	-6.01834(3)	-6.0320(2)	-6.0232(1)	-6.0349(3)

TABLE I. VMC and DMC energies at different system size and the thermodynamic limit obtained using J_F and J_C two-body el-el Jastrow term. The energy at the infinite system size limit is obtained using the linear extrapolation (Fig. 2).

The Jastrow term in the trial wavefunction is responsible for the dynamic correlation between electrons and includes a homogeneous two-body factor J_{2b} , which is a function of the relative distance between two electrons, and a non-homogeneous three-body term J_{3b} which is a function of the atomic position, defined as:

$$J_{2b} = \exp\left(\sum_{i < j} u(r_{ij})\right) \quad (3)$$

$$J_{3b} = \exp\left(\sum_{i < j} f(\mathbf{r}_i, \mathbf{r}_j)\right); f(\mathbf{r}_i, \mathbf{r}_j) = \sum_{ablm} g_{ilm}^{ab} \chi_{al}(\mathbf{r}_i) \chi_{bm}(\mathbf{r}_j) \quad (4)$$

where g_{ilm}^{ab} are optimizable parameters. The three-body electron-ion-electron is defined by the diagonal matrix elements g^{aa} . The off-diagonal g^{ab} , $a \neq b$ matrix elements define the four-body electron-ion-electron-ion terms that were not used in our study. $f(\mathbf{r}_i, \mathbf{r}_j)$ is a two-electron coordinate function expanded using one-particle basis sets, i, j are electron indices, and r_{ij} are electron-electron distances. We used two different forms for the two-body homogeneous part $u_F = r/(2(1+ar))$ [51] and $u_C = \frac{b}{2}(1 - \exp(-r/b))$ [52], where r is the relative distance between two electrons, a and b are variational parameters. For Jastrow single-particle orbitals, we used uncontracted Gaussian basis sets of $3s3p1d$ and $3s2p$ for Fe and Se, respectively. The DMC energies are obtained using the time step 0.01 a.u., the 3200 number of walkers (configurations) and the locality approximation for the pseudopotential[53].

III. NUMERICAL RESULTS

Figure 1 shows the difference between the VMC and DFT energies during the last 100 optimization steps out of several hundreds of optimization iterations. The number of optimization steps was increased by system size. The results of the WF optimization procedure are shown for three system sizes and two-body Jastrow forms of u_F and u_C , which are defined in Section II. Only the coefficients of Jastrow factor were optimized in Fig. 1(a), while Fig. 1(b) shows the results for full optimization of the Jastrow term. The Jastrow term and the Slater determinant were optimized simultaneously in Fig. 1(c). The VMC and DMC energies obtained by the wave functions JDF and JSD as a function of the system size are shown in Fig. 2. All the results of Figs. 1 and 2 were obtained for double layer FeSe with in-plane iron-iron bond length 3.689 Å and interlayer separation 5.83 Å, which is the optimized value predicted by our DMC results (Fig. 3). The ground state energy of the system at the infinite system size limit is obtained by using linear extrapolation of the VMC and DMC energies as a function of $1/N$, where N is the number of electrons in the simulation cell. The values of VMC and DMC energies at each system size and the thermodynamic limit are presented in Table I.

The nearly degenerate electronic configurations close to the minimum of VMC and DMC energy curves (Fig. 3) suggest strong static correlation and multi-reference character of the system driven by strong el-el interactions. This implies the importance of using the multideterminant trial wave function to accurately describe the ground-state electronic structure. To investigate this behavior further, we increased the number of Fe- d orbitals in the single-particle basis set of the Slater determinant and the Jastrow factor. The VMC and DMC energies of the double layer FeSe, which are calculated using the determinant and Jastrow base set of $8s6pnd1f$, ($n = 4, 6$) and $3s3pnd$, ($n = 1, 3$), respectively, for the iron atom, are listed in table II. The energies are obtained for double-layer FeSe with Fe-Fe bond length of 3.689 Å and interlayer separation of 5.83 Å. The dynamic correlation captured by the Jastrow factor is weaker than the static correlation. Hence, increasing the number of Fe- d orbitals in the slater determinant basis set improves the ground-state energy more than the Jastrow basis set. Compared with DMC, the VMC energies are more affected by the number of Fe- d orbitals in the base set. More importantly, full optimization of the wave function reduces the effect of number of Fe- d orbitals in the basis set as shown by the $DMC-JSD$ energies (tab. II). Comparing the $DMC-JSD$ energies of the smallest and largest basis sets shows that reaching the mHa/el accuracy is possible by full optimization of the wave function and without increasing the size of the basis set.

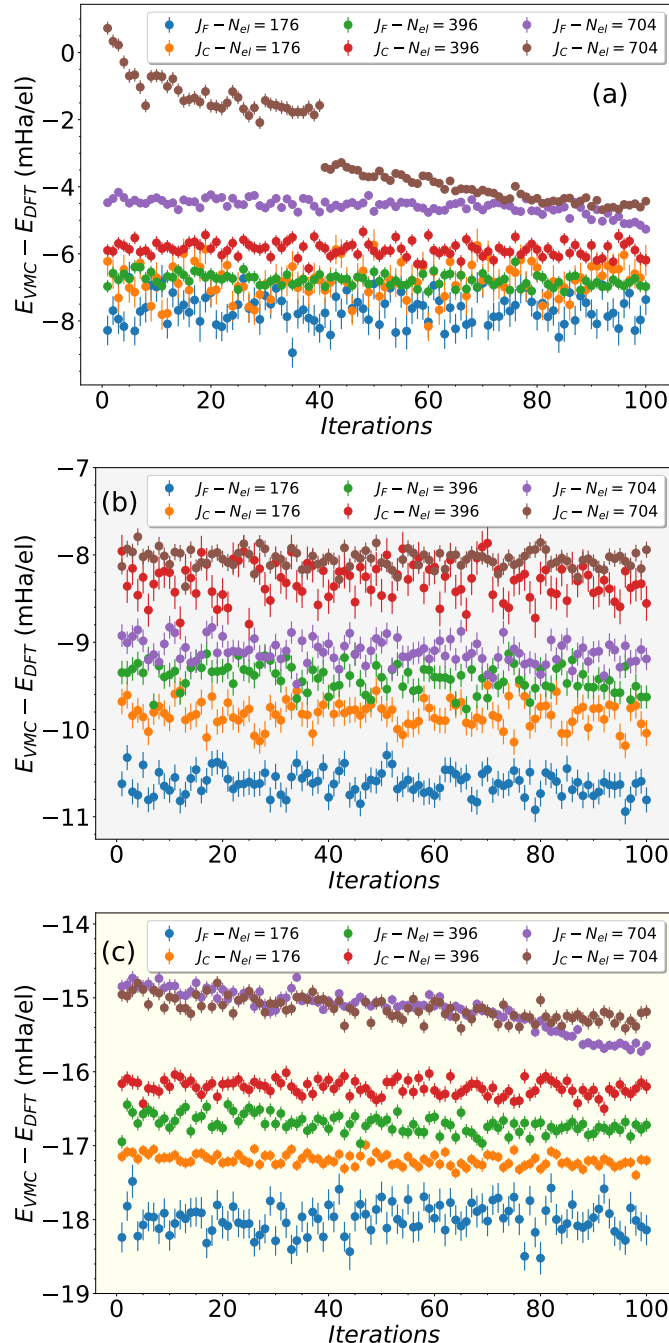


FIG. 1. The difference between VMC and DFT energies as a function of the number of optimization iteration. (a) Only the coefficients of the Jastrow terms are optimised, (b) The exponent and Coefficients of the Jastrow term are optimized simultaneously, (c) The Jastrow and Slater determinat are optimised. Two Jastrow forms of u_F and u_C were used. Only the last one hundred optimization steps are shown. Three system sizes with number of electrons in simulation cell $N_{el} = 176, 396, 704$ were considered.

We calculated the VMC and DMC ground state energy curve of double-layer FeSe as a function of interlayer separation. We considered the experimental inplane iron-iron bond length of 3.689 Å and the stretched iron-iron bond length of 4.233 Å. The energy curves, which are obtained using the *JDFT* and *JSD* wave functions, are illustrated in Fig. 3. The DFT, VMC, and DMC energy values of the data points in Fig. 3, are listed in tables. III and IV. All energy data points in Fig. 3 are obtained using the basis set $8s6p4d1f/3s3p1d$ for the iron atom.

The VMC and DMC correlation energy of the double layer FeSe as a function of the distance between the layers

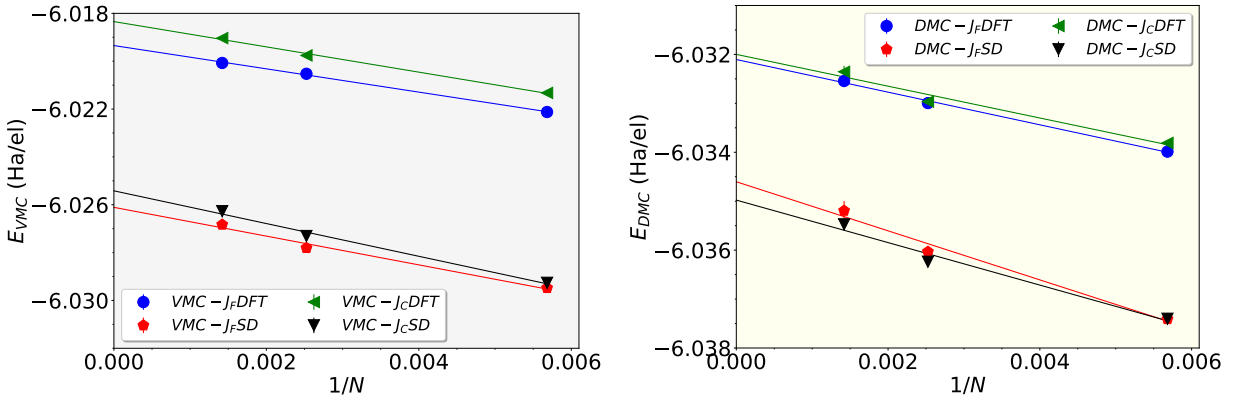


FIG. 2. VMC E_{VMC} (left panel) and DMC E_{DMC} (right panel) energy of double layer FeSe as a function of $1/N$, where N is the number of electrons in the simulation cell, obtained using J_F and J_C two-body el-el Jastrow factors.

Basis	VMC-JDFT	VMC-JSD	DMC-JDFT	DMC-JSD
6d-J3d	-6.028753(6)	-6.032268(5)	-6.03596(1)	-6.03775(1)
6d-J1d	-6.027060(6)	-6.030781(5)	-6.035886(9)	-6.037612(8)
4d-J3d	-6.022436(6)	-6.030045(5)	-6.034025(9)	-6.037344(8)
4d-J1d	-6.022123(6)	-6.029479(5)	-6.033987(9)	-6.037408(8)

TABLE II. VMC and DMC energies of double layer FeSe obtained using determinant single-particle orbital basis set $8s6pnd1f$; ($n = 4, 6$) and $6s4p2d$ for Fe and Se , respectively, and Jastrow orbital $3s3pnd$, ($n = 1, 3$) and $3s2p$ for Fe and Se , respectively. On the number of d orbital is listed in the first column. Energies are in Ha/el and are calculated using two-body Jastrow u_F . The energies are obtained for double-layer FeSe with Fe-Fe bond length 3.689 Å and the distance between layers 5.83 Å.

$d(\text{\AA})$	HF	DFT	$VMC - JDFT$	$VMC - JSD$	$DMC - JDFT$	$DMC - JSD$
4.27	-5.3439236	-6.0112733	-6.021038(6)	-6.027753(5)	-6.033048(9)	-6.035778(8)
4.79	-5.3472775	-6.0118530	-6.021618(6)	-6.028438(5)	-6.033569(9)	-6.036546(8)
5.16	-5.3499789	-6.0121258	-6.022014(6)	-6.028825(5)	-6.034169(9)	-6.037144(8)
5.53	-5.3518114	-6.0118895	-6.021896(6)	-6.028921(5)	-6.034165(9)	-6.037319(8)
5.83	-5.3531499	-6.0114938	-6.022123(6)	-6.029479(5)	-6.033987(9)	-6.037408(8)
6.09	-5.3538347	-6.0110016	-6.020785(6)	-6.029394(5)	-6.033591(9)	-6.036983(8)
6.27	-5.3542681	-6.0105423	-6.020053(6)	-6.028906(5)	-6.033299(9)	-6.036674(8)

TABLE III. Ground state energy of double layer FeSe as a function of interlayer separation (d) in Ha/el. The energies are obtained using a simulation cell with 176 electrons, two-body Jastrow term J_F , and Fe-Fe bond-length 3.651 Å.

$d(\text{\AA})$	HF	DFT	$VMC - JDFT$	$VMC - JSD$	$DMC - JDFT$	$DMC - JSD$
3.39	-5.3454731	-6.008139	-6.018283(6)	-6.025481(6)	-6.03039(5)	-6.03332(5)
3.81	-5.3497955	-6.009011	-6.019812(6)	-6.027055(5)	-6.03180(5)	-6.03487(4)
4.23	-5.3522866	-6.008861	-6.020030(6)	-6.027989(5)	-6.03202(5)	-6.03571(4)
4.66	-5.3539755	-6.008240	-6.019513(6)	-6.027859(5)	-6.03177(5)	-6.03574(4)
5.08	-5.3550693	-6.007422	-6.018945(6)	-6.027605(5)	-6.03137(5)	-6.03556(5)
5.50	-5.3557858	-6.006575	-6.018307(6)	-6.027461(5)	-6.03089(5)	-6.03552(5)
5.93	-5.3561037	-6.005549	-6.017355(6)	-6.026636(5)	-6.03033(5)	-6.03485(5)
6.35	-5.3559713	-6.004349	-6.016710(6)	-6.026427(5)	-6.02962(5)	-6.03455(5)
6.69	-5.3555844	-6.003223	-6.015909(6)	-6.025875(5)	-6.02874(5)	-6.03386(4)
6.98	-5.3552118	-6.002385	-6.014770(6)	-6.024265(5)	-6.02820(5)	-6.03273(5)

TABLE IV. Ground state energy of double layer FeSe as a function of interlayer separation (d) in Ha/el. The energies are obtained using a simulation cell with 176 electrons, two-body Jastrow term J_F , and Fe-Fe bond-length 4.233 Å.

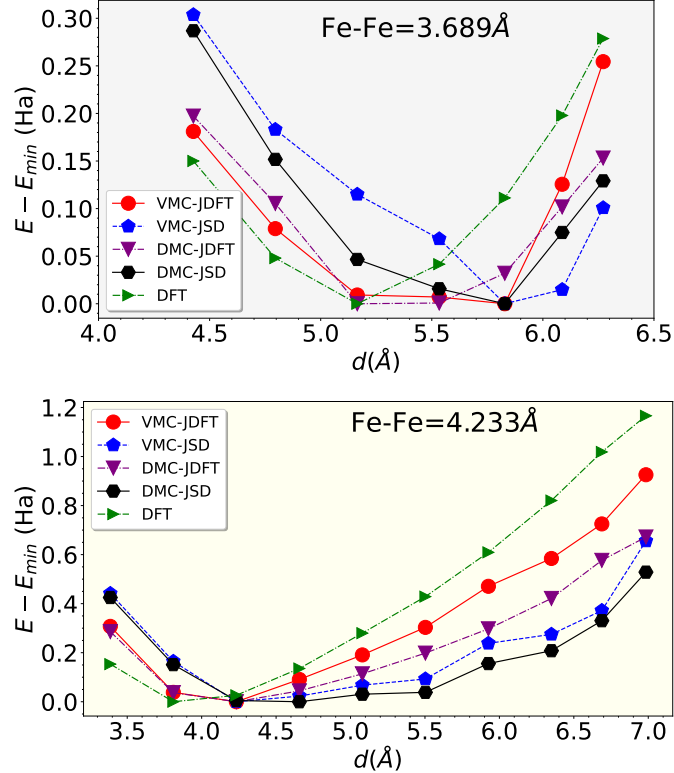


FIG. 3. Energy of double-layer FeSe with respect to the minimum energy E_{min} as a function of separation between layers. The energies are calculated using VMC and DMC with JDFT and JSD wave functions and also DFT. The energy curves are obtained for double-layer FeSe with Fe-Fe bond length 3.689\AA (top panel) and 4.233\AA (bottom panel).

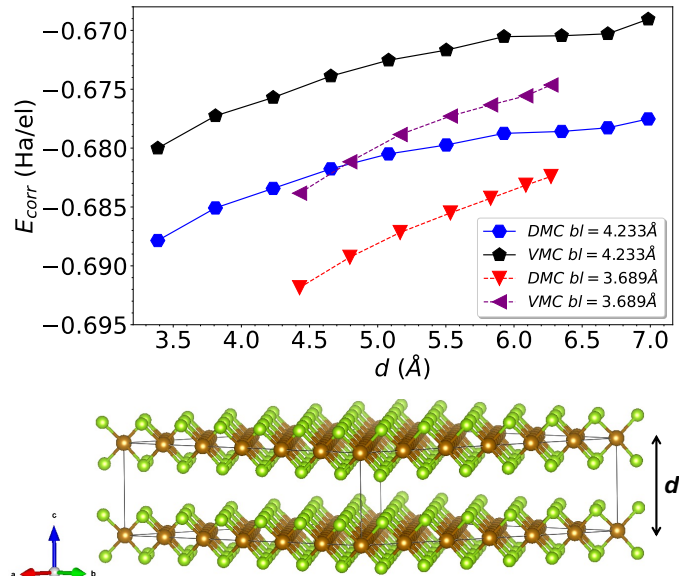


FIG. 4. (Top panel) Correlation energy per electron for double layer FeSe as a function of interlayer separation. The energies are obtained using VMC and DMC with *JSD* wave function for two Fe-Fe bond-length (*bl*) 3.689 and 4.233 \AA . (Bottom panel) Geometry of double layer FeSe in which d is the distance between the center of mass of each layer. Fe and Se atoms are brown and green spheres, respectively.

is shown in Fig. 4. The results were calculated using the wave function *JSD* which is more accurate than *JDFT*. The correlation energies were obtained for two different Fe-Fe bond lengths 3.689 and 4.233 Å and system size 176 electrons.

IV. DISCUSSION

We specifically focused on optimizing the trial wave function for each system size and lattice parameter before performing the final VMC and DMC simulations. The trial wave function is crucial in QMC simulations because it directly affects the accuracy, efficiency, and stability of the simulations, as it serves as a guiding function for importance sampling in DMC, which modifies the diffusion equation to improve convergence. A properly optimized trial wave function can lead to large statistical fluctuations, making it difficult to obtain precise results. Optimizing the trial wave function reduces variance, leading to faster and more stable simulations. We systematically optimized the trial wave function by following three steps: (I) The Jastrow coefficients and the two-body term u were optimized, as shown in Fig. 1(a). In this step, depending on the size of the system, $\sim 4 - 8$ mHa / el VMC energy obtained with respect to DFT. (II) The Jastrow function was fully optimized (Fig. 1(b)) and the wave function was called *JDFT*. The energy difference between VMC and DFT is $\sim 8 - 11$ mHa/el, depending on the system size. (III) The Jastrow and Slater determinant were optimized simultaneously and the wave function was named *JSD*. Since the FS errors normally increase by the number of electrons in the simulation cell, the VMC energy gain with respect to DFT is smaller for larger systems. We found that following these three steps in order, meaning that the well-optimized wave function at the end of each step is used as the initial wave function for the next step, is required to reach an accuracy of mHa/el and avoid local minima.

Performing QMC simulations in a finite supercell with periodic boundary conditions (PBC) suffers from finite-size (FS) errors [54]. The main source of FS errors includes (i) the single-particle FS effect, which is because of the discrete k -point sampling in a finite simulation cell, the electron momentum states are quantized leading to errors in kinetic and exchange energies. (ii) Coulomb FS error, which is due to the issue that the long-range Coulomb interaction is artificially truncated by PBCs and therefore self-interaction and electrostatic image effects distort the interaction energy. (iii) Many-body correlation FS error mainly driven by the absence of long-wavelength collective excitations in small simulation cells. To correct FS errors, we used the Ewald summation and FS scaling extrapolation as shown in Fig. 2. The single-particle FS errors in the kinetic energy part of Hamiltonian can be corrected by twist averaging [54]. The almost perfect linear behavior of the VMC and DMC energies as a function of $1/N$ suggests that the single-particle FS errors are relatively small in our simulations.

Comparison of the difference between *JDFT* and *JSD* energies and DFT indicates that substantial energy gain can be obtained by fully optimizing the trial WF. The results indicate that the quality of the VMC and DMC energies strongly depends on the trial wave function. The fixed node (FN) approximation, used in the DMC calculations, restricts the many-body WF to having the same nodal surface as the trial WF initially obtained by DFT-LDA. This prevents walkers from crossing into regions of opposite sign, avoiding the sign problem but introducing bias. The calculated DMC energy is an upper bound to the true ground-state energy, and the accuracy of the results depends on the quality of the WF. The effect of FN approximation on DMC energies of iron-based compounds can be large because of the complexity of the nodal surface. As our results show, the FN-DMC energy obtained using *JDFT* is only as good as the trial wave function obtained by LDA-DFT, which inadequately captures strong electron correlations.

Our VMC and DMC energies for double-layer FeSe at equilibrium configuration are obtained using two forms for two-body Jastrow functions. The pair correlation function $u_F(r)$ is more suitable in atomic chemical bond separation, while $u_C(r)$, which is large and positive for $r = 0$ and goes to zero as $r \rightarrow \infty$, is useful when the atoms are at a distance greater than the variational parameter b . In principle, the VMC energies obtained from the two-body Jastrow $u_F(r)$ and $u_C(r)$ should agree with statistical noise, as our results show (Fig. 2). The VMC energies obtained by the wave function *JSD* and $u_F(r)$ and $u_C(r)$ agree completely with the error bars. We propose the idea that using two different forms for the two-body Jastrow term and finding a good agreement between the VMC energies can be used as a test for the accuracy of wave function optimization. The DMC energies are almost independent of the form of Jastrow functions, as our results show (Fig. 2), since the nodal surface is not directly affected by the Jastrow function. The DMC correlation energy of double layer FeSe at equilibrium obtained using the *JDFT* and *JSD* wave functions is 0.6789(2) and 0.6817(3) Ha/el, respectively. The correlation energy of moderately correlated transition metals such as Fe and Ni is $\sim 0.2 - 0.4$ Ha/el [55], while the strongly correlated transition metal oxides such as FeO and NiO have the correlation energy of $\sim 0.5 - 1.0$ Ha/el [40, 56]. Our DMC results indicate that the el-el correlation energy of double-layer FeSe is in the strongly correlated range. The bulk FeSe with the tetragonal crystal structure is metallic [57]. Hence, it would be expected that electrons are moderately correlated. Our DMC results predict that the three- to two-dimensional transition increases the el-el correlation energy in FeSe. Therefore, the localised Hubbard U parameter, widely used in DFT+ U simulations for transition metal compounds, for double-layer FeSe is

larger than the one for crystal FeSe.

Comparison of the energy curves as a function of the distance between FeSe layers (Fig. 3) shows that the optimized separation between FeSe layers decreases as the iron-iron bond length stretches. The energy curves *VMC-JDFT* and *DMC-JDFT* for Fe-Fe = 3.689 Å show a degeneracy near the minimum which can be relatively removed by optimizing the Slater determinant as the energy curves *VMC-JSD* and *DMC-JSD* display. However, this degeneracy vicinity of the energy minimum becomes more pronounced with increasing iron-iron bond length, and cannot be removed by optimizing the Slater determinant as shown by the energy curves *VMC-JSD* and *DMC-JSD* for Fe-Fe = 4.233 Å. These results indicate that stretching the bond length in the strongly correlated double-layer FeSe system enlarges the static correlation driven by the localization of electrons of the iron d-orbital. Hence, using multideterminant or at least using better single-particle orbitals than DFT-LDA such as multiconfigurational self-consistent field orbitals may improve the description of the static correlation effects in this system.

The VMC and DMC results with the wave function *JSD* show that the absolute value of the correlation energy decreases as the distance between the layers of FeSe double-layer increases (Fig. 4). Within the interlayer separation range studied, the absolute value of the correlation energy of the FeSe double layer with a Fe-Fe bond length 3.689 Å at fixed d is higher than in the system with Fe-Fe bond length 4.233 Å. However, the correlation energy of the system with the Fe-Fe bond length 3.689 Å decreases faster with d than the stretched system. The extrapolation of our results predicts that the correlation energy of two systems at $d > 7$ Å may cross over. This suggests that in-plane stretch affects the nature of interaction between layers in double-layer FeSe.

ACKNOWLEDGEMENTS

We acknowledge the support of the Leverhulme Trust under the grant agreement RPG-2023-253. S. Azadi and T.D. Kühne acknowledge the computing time provided to them on the high-performance computers Noctua2 at the NHR Center in Paderborn (PC2).

[1] Q. H. Wang, A. Bedoya-Pinto, M. Blei, A. H. Dismukes, A. Hamo, S. Jenkins, M. Koperski, Y. Liu, Q.-C. Sun, E. J. Telford, H. H. Kim, M. Augustin, U. Vool, J.-X. Yin, L. H. Li, A. Falin, C. R. Dean, F. Casanova, R. F. Evans, M. Chshiev, A. Mishchenko, C. Petrovic, R. He, L. Zhao, A. W. Tsen, B. D. Gerardot, M. Brotons-Gisbert, Z. Guguchia, X. Roy, S. Tongay, Z. Wang, M. Z. Hasan, J. Wrachtrup, A. Yacoby, A. Fert, S. Parkin, K. S. Novoselov, P. Dai, L. Balicas, and E. J. Santos, The magnetic genome of two-dimensional van der waals materials, *ACS Nano* **16**, 6960 (2022).

[2] M. Gibertini, M. Koperski, A. Morpurgo, and K. Novoselov, Magnetic 2d materials and heterostructures, *Nature nanotechnology* **14**, 408 (2019).

[3] S. Jenkins, L. Rózsa, U. Atxitia, R. F. L. Evans, K. S. Novoselov, and E. J. G. Santos, Breaking through the mermin-wagner limit in 2D van der waals magnets, *Nat. Comm.* **13**, 6917 (2022).

[4] C. Gong and et al, Discovery of intrinsic ferromagnetism in two dimensional van der waals crystals, *Nature* **546**, 265 (2017).

[5] H. Kontani and S. Onari, Orbital-fluctuation-mediated superconductivity in iron pnictides: Analysis of the five-orbital hubbard-holstein model, *Phys. Rev. Lett.* **104**, 157001 (2010).

[6] A. E. Böhmer and A. Kreisel, Nematicity, magnetism and superconductivity in FeSe, *J. Phys.: Condensed Matter* **30**, 023001 (2018).

[7] S. Medvedev, T. M. McQueen, I. A. Troyan, T. Palasyuk, M. I. Eremets, R. J. Cava, S. Naghavi, F. Casper, V. Ksenofontov, G. Wortmann, and C. Felser, Electronic and magnetic phase diagram of β -Fe_{1.01}Se with superconductivity at 36.7 K under pressure, *Nat. Mater.* **8**, 630 (2009).

[8] B. Kang, M. Kim, C. H. Park, and A. Janotti, Mott-insulator state of FeSe as a van der waals 2D material is unveiled, *Phys. Rev. Lett.* **132**, 266506 (2024).

[9] E. Dagotto, Colloquium: The unexpected properties of alkali metal iron selenide superconductors, *Rev. Mod. Phys.* **85**, 849 (2013).

[10] P. Dai, Antiferromagnetic order and spin dynamics in iron-based superconductors, *Rev. Mod. Phys.* **87**, 855 (2015).

[11] B. Huang, M. A. McGuire, A. F. May, D. Xiao, P. Jarillo-Herrero, and X. Xu, Emergent phenomena and proximity effects in two-dimensional magnets and heterostructures, *Nature Materials* **19**, 1276 (2020).

[12] K. Kothapalli, A. Böhmer, W. Jayasekara, B. Ueland, P. Das, A. S. V. Taufour, Y. Xiao, E. Alp, S. Bud'ko, P. Canfield, A. Kreyssig, and A. Goldman, Strong cooperative coupling of pressure-induced magnetic order and nematicity in FeSe, *Nat. Commun.* **7**:12728 **7**, 12728 (2016).

[13] B. Huang, G. Clark, E. Navarro-Moratalla, D. R. Klein, R. Cheng, K. L. Seyler, D. Zhong, E. Schmidgall, M. A. McGuire, D. H. Cobden, W. Yao, D. Xiao, P. Jarillo-Herrero, and X. Xu, Layer-dependent ferromagnetism in a van der waals crystal down to the monolayer limit, *Nature* **546**, 270 (2017).

[14] H. Zhang, T. Pincelli, C. Jozwiak, T. Kondo, R. Ernstorf, T. Sato, and S. Zhou, Angle-resolved photoemission spectroscopy, *Nature Reviews Methods Primers* **2**, 54 (2022).

- [15] L. D. Landau, On the theory of the fermi liquid, Sov. Phys. JETP **35**, 95 (1958).
- [16] S. Azadi, N. Drummond, and S. Vinko, Quantum monte carlo study of the phase diagram of the two-dimensional uniform electron liquid, Phys. Rev. B **110**, 245145 (2024).
- [17] R. Tazai, S. Matsubara, Y. Yamakawa, S. Onari, and H. Kontani, Rigorous formalism for unconventional symmetry breaking in fermi liquid theory and its application to nematicity in FeSe, Phys. Rev. B **107**, 035137 (2023).
- [18] A. V. Chubukov, M. Khodas, and R. M. Fernandes, Superconductivity, and spontaneous orbital order in iron-based superconductors: Which comes first and why?, Phys. Rev. X **6**, 041045 (2016).
- [19] Y. Yamakawa, S. Onari, and H. Kontani, Nematicity and magnetism in FeSe and other families of Fe-based superconductors, Phys. Rev. X **6**, 021032 (2016).
- [20] S. Onari, Y. Yamakawa, and H. Kontani, Sign-reversing orbital polarization in the nematic phase of FeSe due to the symmetry breaking in the self-energy, Phys. Rev. Lett. **116**, 227001 (2016).
- [21] R. Fernandes, A. Chubukov, and J. Schmalian, What drives nematic order in iron-based superconductors?, Nat. Phys. **10**, 97 (2014).
- [22] T. M. McQueen, A. J. Williams, P. Stephens, J. Tao, Y. Zhu, V. Ksenofontov, F. Casper, C. Felser, and R. J. Cava, Tetragonal-to-orthorhombic structural phase transition at 90K in the superconductor $Fe_{1.01}Se$, Phys. Rev. Lett. **103**, 057002 (2009).
- [23] H. Alloul, J. Bobroff, M. Gabay, and P. J. Hirschfeld, Defects in correlated metals and superconductors, Rev. Mod. Phys. **81**, 45 (2009).
- [24] M. Yi, D. H. Lu, R. Yu, S. C. Riggs, J.-H. Chu, B. Lv, Z. K. Liu, M. Lu, Y.-T. Cui, M. Hashimoto, S.-K. Mo, Z. Hussain, C. Chu, I. R. Fisher, Q. Si, and Z.-X. Shen, Observation of temperature-induced crossover to an orbital-selective mott phase in $AFe_{2-y}Se_2$ ($A=K, Rb$) superconductors, Phys. Rev. Lett. **110**, 067003 (2013).
- [25] Z. Yin, K. Haule, and G. Kotliar, Kinetic frustration and the nature of the magnetic and paramagnetic states in iron pnictides and iron chalcogenides, Nat. Mater. **10**, 932 (2011).
- [26] M. Ma, P. Bourges, Y. Sidis, Y. Xu, S. Li, B. Hu, J. Li, F. Wang, and Y. Li, Prominent role of spin-orbit coupling in FeSe revealed by inelastic neutron scattering, Phys. Rev. X **7**, 021025 (2017).
- [27] S. Azadi, M. Bahramy, and T. Kühne, Electron correlation effects and spin-liquid state in the herbertsmithite kagome lattice, Phys. Rev. Res. **7**, 013165 (2025).
- [28] F.-C. Hsu, J.-Y. Luo, K.-W. Yeh, T.-K. Chen, T.-W. Huang, P. M. Wu, Y.-C. Lee, Y.-L. Huang, Y.-Y. Chu, D.-C. Yan, and M.-K. Wu, Superconductivity in the PbO-type structure α -FeSe, Proc. Nat. Acad. Sci. **105**, 14262 (2008).
- [29] Z. Wang, X.-G. Zhao, R. Koch, S. J. L. Billinge, and A. Zunger, Understanding electronic peculiarities in tetragonal FeSe as local structural symmetry breaking, Phys. Rev. B **102**, 235121 (2020).
- [30] H. Okabe, N. Takeshita, K. Horigane, T. M. T, and J. Akimitsu, Pressure-induced high- T_c superconducting phase in FeSe: correlation between anion height and T_c , Phys. Rev. B **81**, 205119 (2010).
- [31] J. M. Tomczak, M. van Schilfgaarde, and G. Kotliar, Many-body effects in iron pnictides and chalcogenides: Nonlocal versus dynamic origin of effective masses, Phys. Rev. Lett. **109**, 237010 (2012).
- [32] X. Long, S. Zhang, F. Wang, and Z. Liu, A first-principle perspective on electronic nematicity in FeSe, Npj Quantum Mater. **5**, 50 (2020).
- [33] Y. Ding, M. Zeng, Q. Zheng, J. Zhang, D. Xu, W. Chen, C. Wang, S. Chen, Y. Xie, Y. Ding, S. Zheng, J. Zhao, P. Gao, and L. Fu, Bidirectional and reversible tuning of the interlayer spacing of two-dimensional materials, Nat. Comm. **12**, 5886 (2021).
- [34] J. Kolorenč, S. Hu, and L. Mitas, Wave functions for quantum monte carlo calculations in solids: Orbitals from density functional theory with hybrid exchange-correlation functionals, Phys. Rev. B **82**, 115108 (2010).
- [35] J. Kolorenč and L. Mitas, Applications of quantum monte carlo methods in condensed systems, Reports on Progress in Physics **74**, 026502 (2011).
- [36] M. Dubecky, L. Mitas, and P. Jurecka, Noncovalent interactions by quantum monte carlo, Chemical Reviews **116**, 5188 (2016).
- [37] J. Kolorenč and L. Mitas, Quantum monte carlo calculations of structural properties of FeO under pressure, Phys. Rev. Lett. **101**, 185502 (2008).
- [38] B. Busemeyer, M. Dagrada, S. Sorella, M. Casula, , and L. K. Wagner, Competing collinear magnetic structures in superconducting FeSe by first-principles quantum monte carlo calculations, Phys. Rev. B **94**, 035108 (2016).
- [39] C. J. Umrigar, J. Toulouse, C. Filippi, S. Sorella, and R. G. Hennig, Alleviation of the fermion-sign problem by optimization of many-body wave functions, Phys. Rev. Lett. **98**, 110201 (2007).
- [40] W. M. C. Foulkes, L. Mitas, R. J. Needs, and G. Rajagopal, Quantum monte carlo simulations of solids, Rev. Mod. Phys. **73**, 33 (2001).
- [41] F. Becca and S. Sorella, *Quantum Monte Carlo approaches for correlated systems* (Cambridge University, Cambridge, UK, 2017).
- [42] J. B. Anderson, Quantum chemistry by random walk., J. Chem. Phys. **65**, 4121 (1976).
- [43] M. Marchi, S. Azadi, M. Casula, and S. Sorella, Resonating valence bond wave function with molecular orbitals: Application to first-row molecules, J. Chem. Phys. **131**, 154116 (2009).
- [44] K. Nakano, C. Attaccalite, M. Barborini, L. Capriotti, M. Casula, E. Coccia, M. Dagrada, C. Genovese, Y. Luo, G. Mazzola, A. Zen, and S. Sorella, TurboRVB: A many-body toolkit for ab initio electronic simulations by quantum monte carlo, J. Chem. Phys. **152**, 204121 (2020).
- [45] S. Azadi, R. Singh, and T. D. Kühne, Resonating valence bond quantum monte carlo: Application to the ozone molecule, Int. J. Quantum Chem. **115**, 1673 (2015).

- [46] B. P. Pritchard, D. Altarawy, B. Didier, T. D. Gibson, and T. L. Windus, A new basis set exchange: An open, up-to-date resource for the molecular sciences community, *J. Chem. Inf. Model.* **59**, 4814 (2019).
- [47] A. Annaberdiyev, G. Wang, C. A. Melton, M. C. Bennett, L. Shulenburger, and L. Mitas, A new generation of effective core potentials from correlated calculations: 3d transition metal series, *J. Chem. Phys.* **149**, 134108 (2018).
- [48] M. C. Bennett, C. A. Melton, A. Annaberdiyev, G. Wang, L. Shulenburger, and L. Mitas, A new generation of effective core potentials for correlated calculations, *J. Chem. Phys.* **147**, 224106 (2017).
- [49] S. Azadi, C. Cavazzoni, and S. Sorella, Systematically convergent method for accurate total energy calculations with localized atomic orbitals, *Phys. Rev. B* **82**, 125112 (2010).
- [50] J. P. Perdew and A. Zunger, Self-interaction correction to density-functional approximations for many-electron systems, *Phys. Rev. B* **23**, 5048 (1981).
- [51] S. Fahy, X. W. Wang, and S. G. Louie, Variational quantum monte carlo nonlocal pseudopotential approach to solids: Formulation and application to diamond, graphite, and silicon, *Phys. Rev. B* **42**, 3503 (1990).
- [52] D. M. Ceperley, Ground state of the fermion one-component plasma: A monte carlo study in two and three dimensions, *Phys. Rev. B* **18**, 3126 (1978).
- [53] M. Casula, Beyond the locality approximation in the standard diffusion monte carlo method, *Phys. Rev. B* **74**, 161102(R) (2006).
- [54] S. Azadi and W. Foulkes, Systematic study of finite-size effects in quantum monte carlo calculations of real metallic systems, *J. Chem. Phys.* **143**, 102807 (2015).
- [55] A. I. Lichtenstein, M. Katsnelson, and G. Kotliar, Finite-temperature magnetism of transition metals: An ab initio dynamical mean-field theory, *Phys. Rev. Lett.* **87**, 067205 (2001).
- [56] G. Kotliar, S. Y. Savrasov, K. Haule, V. Oudovenko, O. Parcollet, and C. Marianetti, Electronic structure calculations with dynamical mean-field theory, *Rev. Mod. Phys.* **78**, 865 (2006).
- [57] S. Azadi, A. Principi, and M. S. Bahramy, Hot electron-driven structural expansion and magnetic collapse in bilayer FeSe, *Phys. Rev. B* **111**, 115118 (2025).